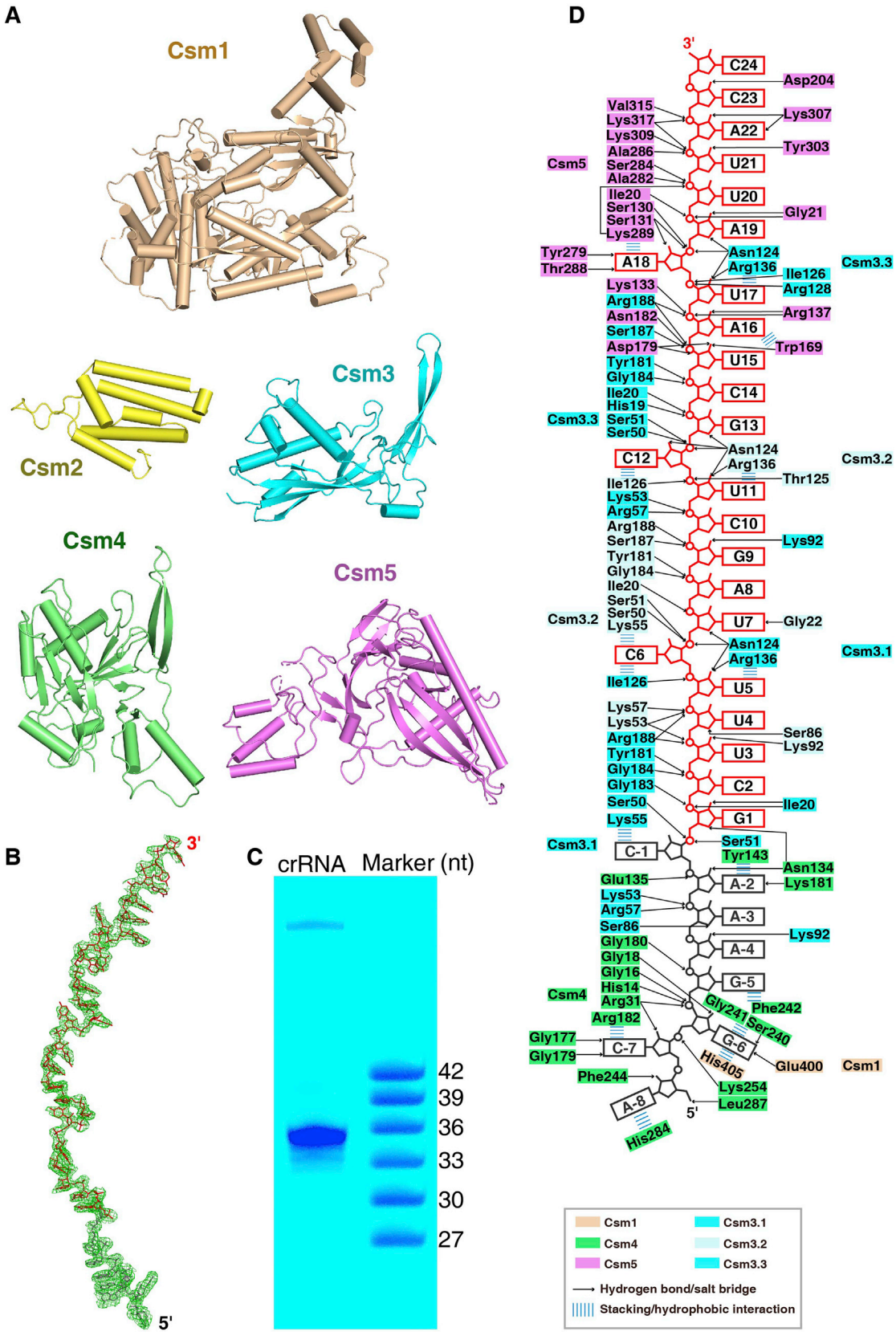

(legend on next page)

Figure S1. Crystal Structure of SthCsm Complex Associate with crRNA, Related to Figure 1

(A) Structures of individual Csm1-5 subunits.

(B) Electron Density of crRNA within SthCsm Complex. Fo-Fc omit map (green color, contoured at 2.0 σ) of the crRNA. The crRNA is shown in stick representation with the space in red and repeat in gray.

(C) Denaturing urea-PAGE gel shows that the length of the crRNA in our SthCsm complex is ~35 nt.

(D) Schematic view of the intermolecular contacts between Csm1-5 subunits and crRNA. Hydrogen bond interactions are indicated by black arrows, and the stacking interactions are shown as blue dashed lines.

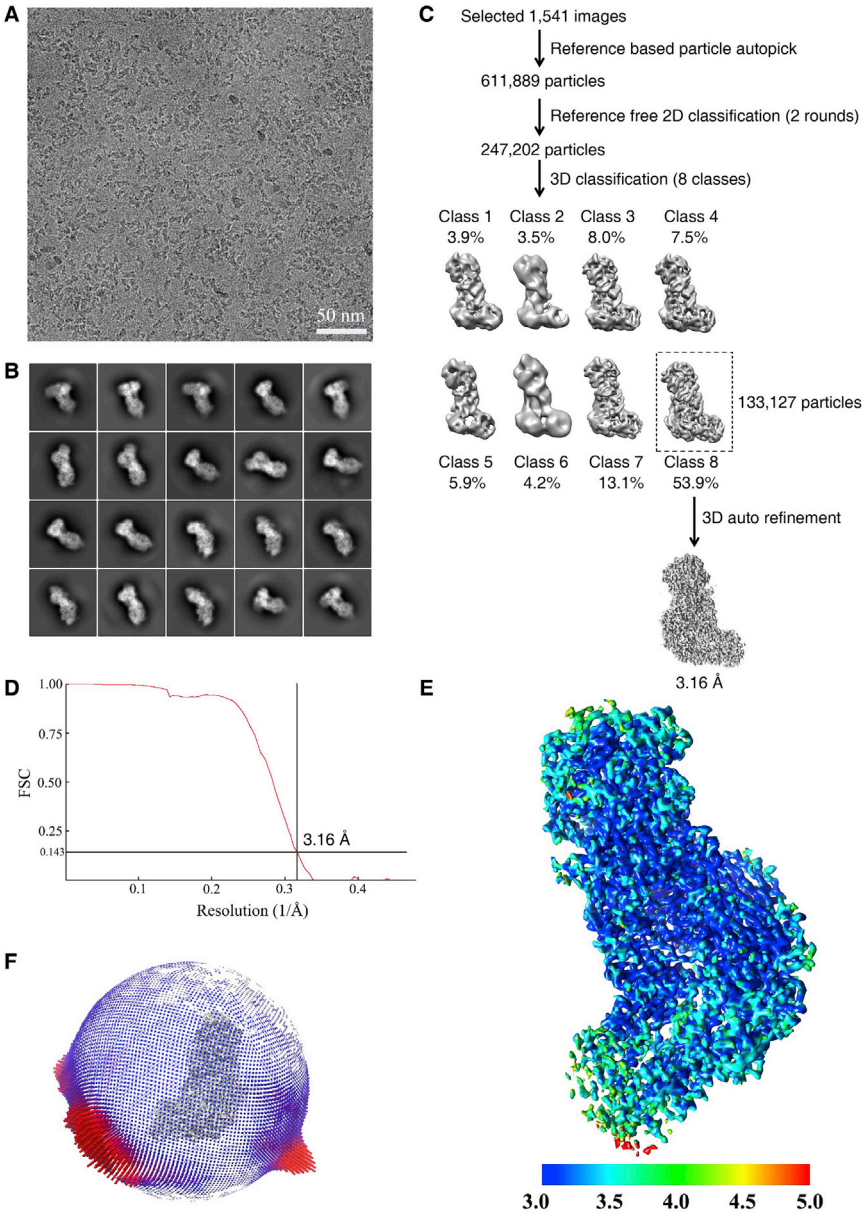

Figure S2. Single Particle Cryo-EM Analysis of Csm-Non-cognate Target RNA Complex, Related to Figure 2

(A) Representative cryo-EM micrograph of Csm-NTR complex.

(B) Representative reference-free 2D-class averages.

(C) Data-processing workflow for the Csm-NTR complex.

(D) The gold standard Fourier shell correlation (FSC) curve of the final density map.

(E) Local resolutions of the cryo-EM map as estimated by RasMap.

(F) Angular distribution of particles included in the final 3D reconstruction.

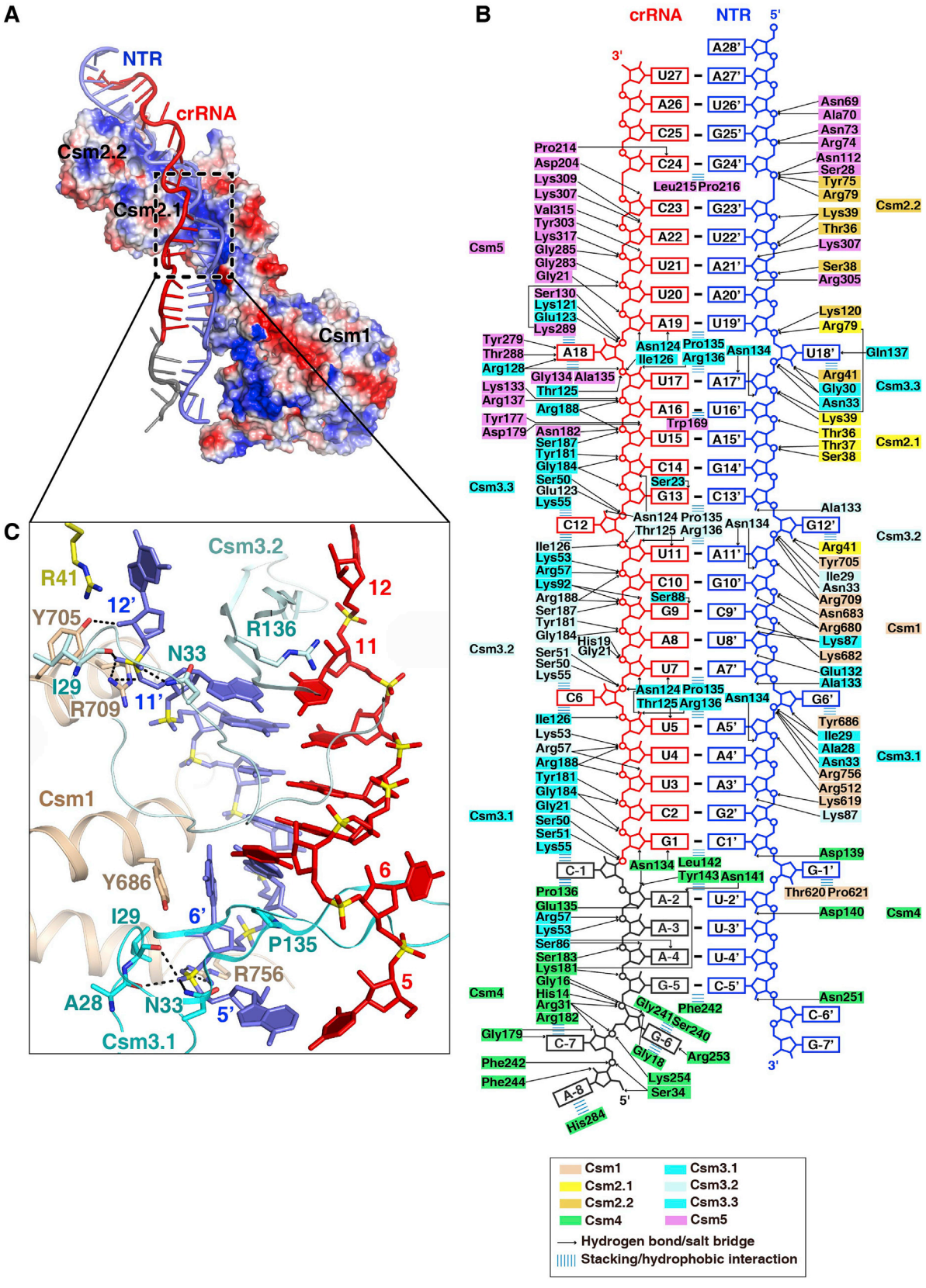

(legend on next page)

Figure S3. Cryo-EM Structure of Csm-Non-cognate Target RNA Complex, Related to Figure 2

(A) Two Csm2 subunit and Csm1 D4 domain form a positive-charged target RNA binding channel. The Csm proteins are shown as a surface representation colored according to electrostatic potential.

(B) Schematic view of the intermolecular contacts between Csm1-5 subunits and crRNA-non-cognate target RNA duplex.

(C) The closed-up view of the interaction between target RNA and Csm.

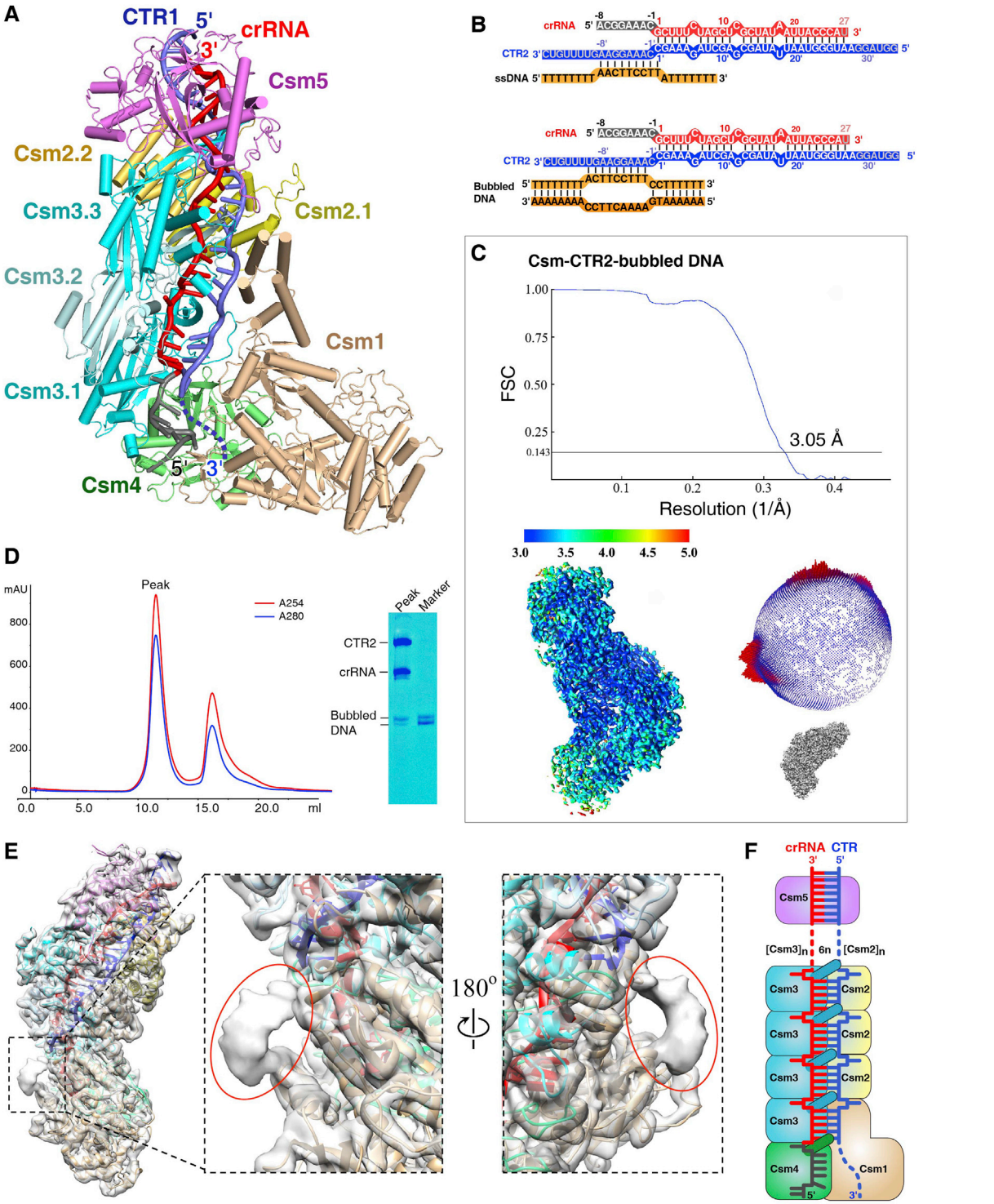

Figure S4. The Cryo-EM Structure of Cognate Target RNA-Bound SthCsm Complex, Related to Figure 3

(A) Cryo-EM structure of SthCsm-crRNA-cognate target RNA complex.

(B) Schematic representation of the crRNA-CTR2 duplex, and the DNA in the complex. The CTR2 is 8 nt longer at the 3′ end compared to the CTR1. DNA is shown in black with orange background. The single stranded DNA is used in the upper panel, and the bubbled DNA is used in the lower panel.

(C) Single particle cryo-EM analysis of the 3.05 Å CTR-bound Csm complex. Top, the gold standard Fourier shell correlation (FSC) curves; Bottom left, local resolutions of the cryo-EM maps estimated by RasMap; Bottom right, angular distribution of particles included in the final 3D reconstruction.

(D) The nucleic acids bound to Csm-CTR2-bubbled DNA complex was checked by denaturing gel.

(legend continued on next page)

(E) Density map of 3′ anti-tag region of target RNA in Csm-CTR2-bubbled DNA complex, which was not built into the model. Extra-density map corresponding 3′ anti-tag region is highlighted in red circles. The central and right panels are enlarged view of the black-dotted boxed area in left panel.
(F) Cartoon scheme of the Csm-crRNA-non-cognate target RNA complex showing that one additional Csm3-Csm2 subcomplex is assembled into the Csm complex with every 6 nt extension of the crRNA.

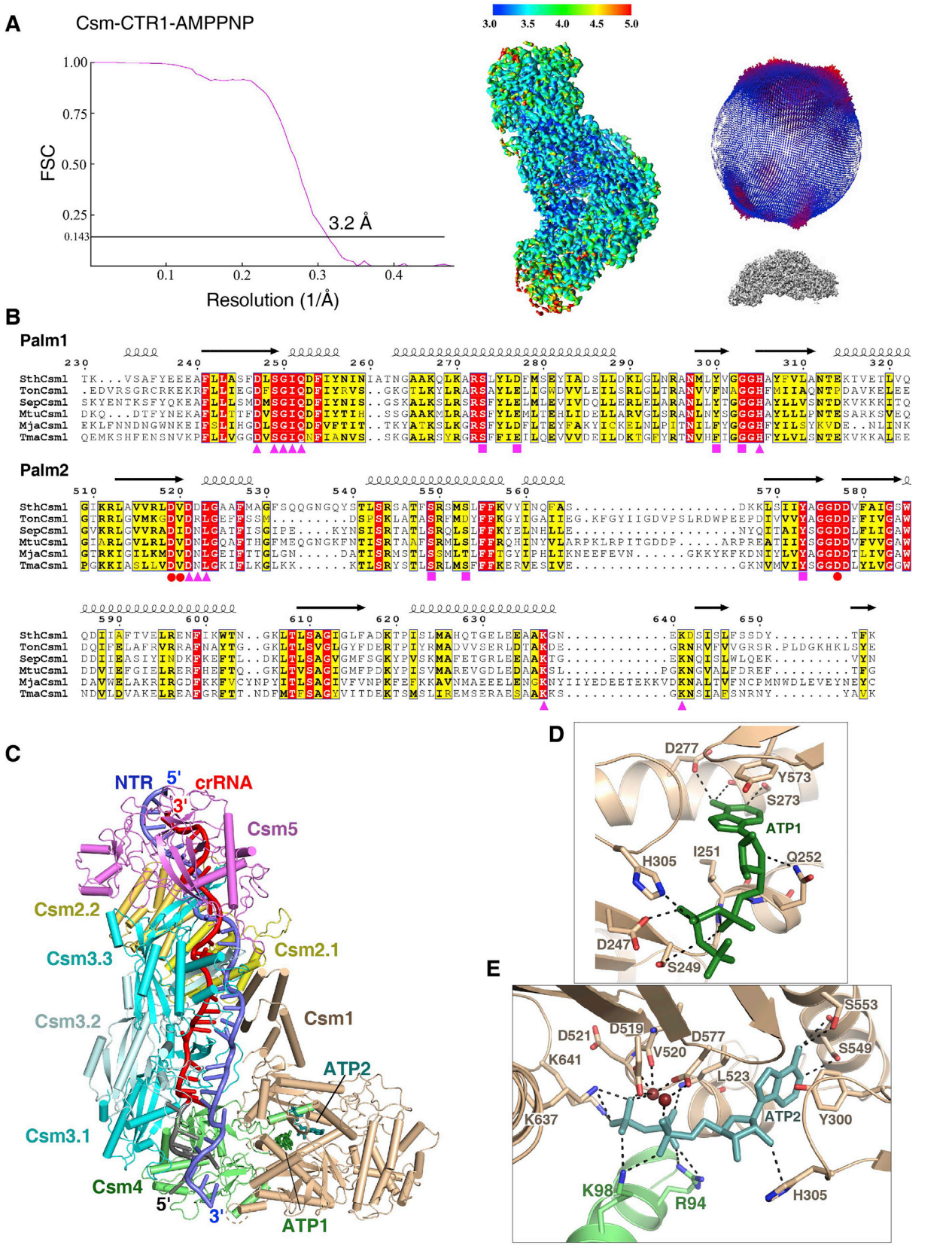

(legend on next page)

Figure S5. The Cryo-EM Structure of Target RNA-Bound SthCsm Complex in the Presence of ATP or AMPPNP, Related to Figures 4 and 5

(A) Single particle cryo-EM analysis of the CTR-bound Csm complex in the presence of AMPPNP.

(B) Sequence alignment of the regions involved in ATP binding within the Palm1 and Palm2 domains. The aligned sequences (Genebank ID and designated gi) are shown in the order of SthCsm1 (*Streptococcus thermophilus* Csm1, gi: 312278321), TonCsm1 (*Thermococcus onnurineus* Csm1, gi: 501567417), SepCsm1 (*Staphylococcus epidermidis* Csm1, gi: 57636542), MtuCsm1 (*Mycobacterium tuberculosis* Csm1, gi: 490009200), MjaCsm1 (*Methanocaldococcus jannaschii* Csm1, gi: 42559943), and TmaCsm1 (*Thermotoga maritime* Csm1, gi: 490183745). The secondary structure of SthCsm1 is shown on top. Conserved residues are shaded in yellow, with essentially invariant residues shown in red. The residues involved in ATP ribose-phosphate backbone binding are shown as magenta triangles, residues involved in sequence specific interaction with ATP are shown by magenta squares, and residues involved in Mg^{2+} binding are shown by red circles.

(C) Cryo-EM structure of Csm in complex with non-cogate RNA in the presence of ATP. Two ATP molecules bound in Csm1 Palm pockets are shown in deep green and teal, respectively.

(D) Detailed view of the ATP1 bound in Palm1 pocket in the non-cognate target RNA-bound Csm complex.

(E) Detailed view of the ATP2 bound in Palm2 pocket in the non-cognate target RNA-bound Csm complex.

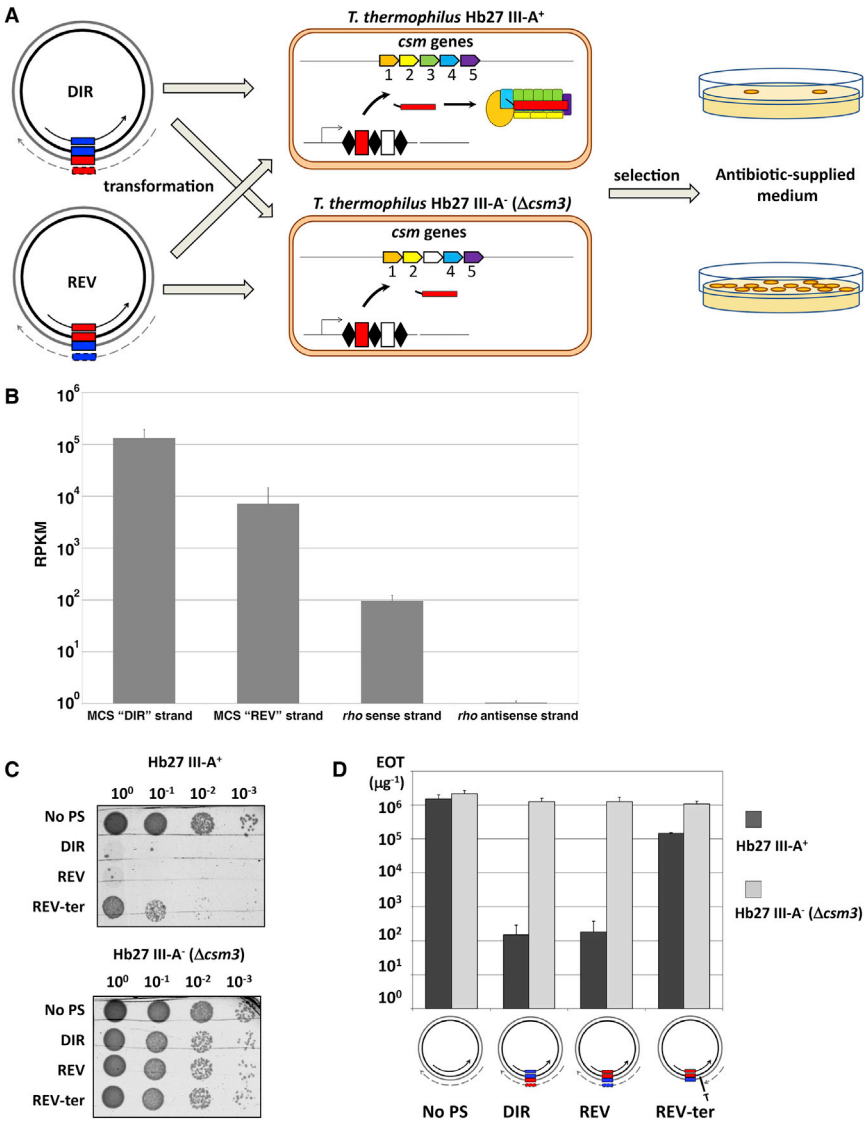

Figure S6. Transcription-Dependent Interference by the Csm Complex Using Plasmid Transformation, Related to Figure 6

(A) A protospacer corresponding to a spacer identified in one of the *T. thermophilus* HB27 Type III CRISPR arrays was cloned into a plasmid vector in either direct ("DIR") or reverse ("REV") orientations. The expected direction of transcription of the protospacer region is indicated by a solid black arrow. Broken gray arrows show counterclockwise transcription from the opposite strand (~2% of clockwise transcription as per RNA-seq analysis). *T. thermophilus* cells with or without a functioning III-A system (III-A^+ and III-A^-) were transformed with plasmids, plated on medium antibiotic-containing medium, before determining the number of colonies formed.

(B) Levels of transcription across the plasmid multiple cloning site (MCS) region in direct and reverse orientations. RPKM were calculated for each strand of pMK18 plasmid MCS ("DIR" strand: value for transcription in direct orientation; "REV" strand: value for transcription in reverse orientation). RPKM values for chromosomal *rho* gene are presented as control. Data are represented as means from three independent experiments with standard deviations shown.

(C) An example of transformation results obtained with control empty vector ("no PS"), plasmids carrying protospacer in both orientations, and a "REV-ter" plasmid containing reverse-oriented protospacer and transcription terminator that decreases protospacer region transcription in counterclockwise direction. Drops of indicated serial dilutions of transformation reactions were deposited on the surface of selective agar. The results for overnight growth at 65°C are shown.

(D) Quantification of data shown on (C). Efficiency of transformation (EOT) values – number of colonies per μg of plasmid DNA are presented. Mean values obtained from three independent experiments and standard deviations are shown.

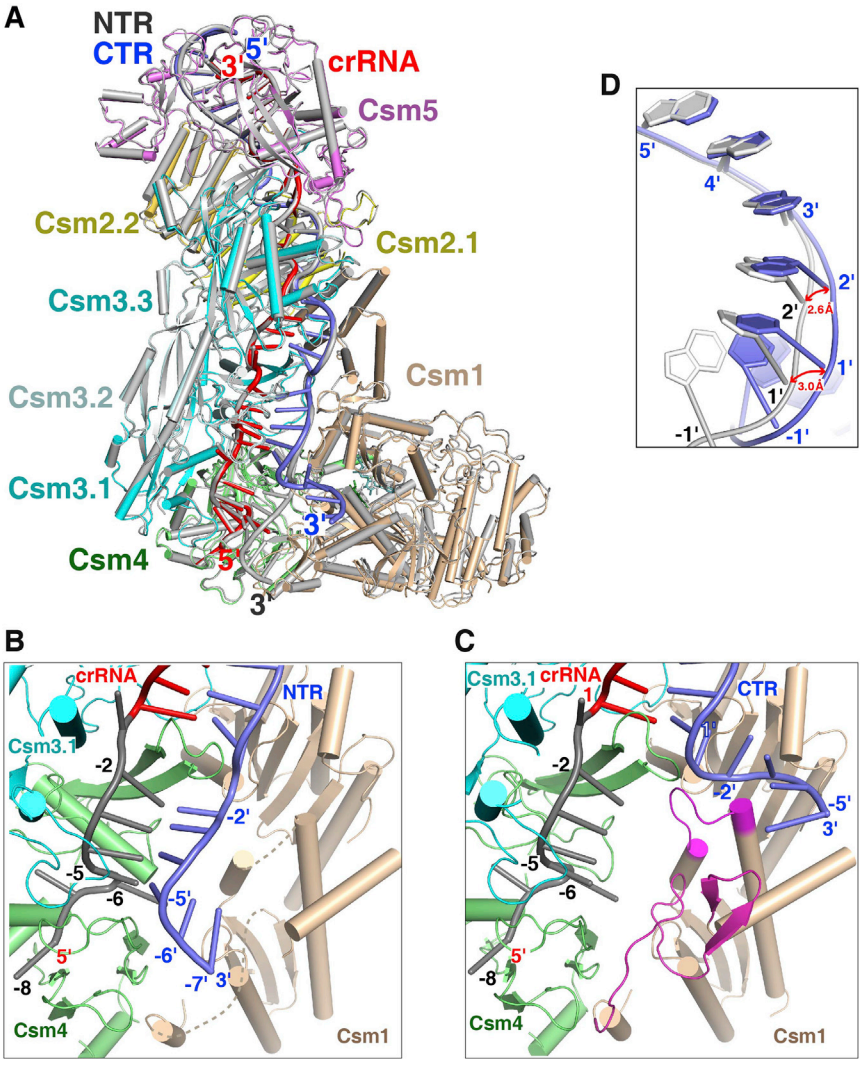

Figure S7. Structural Comparison of Csm in Complex with Either Cognate or Non-cognate Target RNA in the Presence of ATP or AMPPNP, Related to Figure 7

(A) Superposition of cognate and non-cognate target RNA bound Csm complex.

(B) The 3′ anti-tag region of complementary NTR form duplex with 5′ tag of crRNA. The disordered Linker and Loop L1 of Csm1 subunit are shown in wheat dashed lines.

(C) The 3′ anti-tag region of non-complementary CTR swings away from the crRNA. The Linker and Loop L1, which are disordered in the NTR-bound Csm complex, are highlighted in magenta in the CTR-bound Csm complex.

(D) The superposition of the NTR (in gray) and CTR (in blue).